Acat1/Soat1 knockout extends the mutant *Npc1* mouse lifespan and ameliorates functional deficiencies in multiple organelles of mutant cells

Maximillian A. Rogers[a,1], Catherine C. Y. Chang[a,1,2], Robert A. Maue[b], Elaina M. Melton[a], Andrew A. Peden[c], William S. Garver[d], Junghoon Lee[a], Peter Schroen[a], Mitchell Huang[a], and Ta-Yuan Chang[a,2]

Multiple membrane organelles require cholesterol for proper function within cells. The Niemann-Pick type C (NPC) proteins export cholesterol from endosomes to other membrane compartments, including the endoplasmic reticulum (ER), plasma membrane (PM), *trans*-Golgi network (TGN), and mitochondria, to meet their cholesterol requirements. Defects in NPC cause malfunctions in multiple membrane organelles and lead to an incurable neurological disorder. Acyl-coenzyme A:cholesterol acyltransferase 1 (ACAT1), a resident enzyme in the ER, converts cholesterol to cholesteryl esters for storage. In mutant NPC cells, *cholesterol storage still occurs in an NPC-independent manner.* Here we report the interesting finding that in a mutant *Npc1* mouse (*Npc1^nmf*), *Acat1* gene (*Soat1*) knockout delayed the onset of weight loss, motor impairment, and Purkinje neuron death. It also improved hepatosplenic pathology and prolonged lifespan by 34%. In mutant NPC1 fibroblasts, ACAT1 blockade (A1B) increased cholesterol content associated with TGN-rich membranes and mitochondria, while decreased cholesterol content associated with late endosomes. A1B also restored proper localization of syntaxin 6 and golgin 97 (key proteins in membrane trafficking at TGN) and improved the levels of cathepsin D (a key protease in lysosome and requires Golgi/endosome transport for maturation) and ABCA1 (a key protein controlling cholesterol release at PM). This work supports the hypothesis that diverting cholesterol from storage can benefit multiple diseases that involve cholesterol deficiencies in cell membranes.

Niemann-Pick disease type C | acyl-coenzyme A:cholesterol acyltransferase | cholesterol esterification

Niemann-Pick disease type C (NPCD) is a genetically recessive neurodegenerative disorder, caused by mutations in *Npc1* (1) or in *Npc2* (2). Loss of NPC1 or NPC2 function results in the accumulation of cholesterol (3) and various sphingolipid species (4), mainly within late endosomes/lysosomes (LE/LYS). This lipid accumulation occurs in all tissues and results in neurodegeneration and malfunction of liver and lung. The most extensive neuronal death occurs in the cerebellum, with preferential loss of Purkinje neurons. Miglustat, a glycosphingolipid synthesis inhibitor, has demonstrated some efficacy to treat NPCD (5), but it is not approved for NPC therapy in the United States. In addition, intrathecal delivery of 2-hydroxypropyl-β-cyclodextrin, a water-soluble molecule that binds cholesterol, reduces neurological disease progression (6), but its clinical benefit in NPCD patients has yet to be clearly demonstrated. Moreover, high-concentration 2-hydroxypropyl-β-cyclodextrin treatments caused hearing loss in both healthy and NPC mutant animals (7). More recently, several laboratories have explored gene therapy-based approaches as a means to improve the NPC1 disease phenotypes and have produced interesting results (8). Nevertheless, given the current shortage of approved NPCD treatments, it remains a critical need to develop additional potential therapeutic approaches for treating NPCD.

Cholesterol is a lipid molecule essential for cell growth and function. Cells acquire cholesterol through exogenous sources as well as de novo biosynthesis. Exogenous cholesterol enters cells mainly through receptor-mediated endocytosis, followed by distribution to various membrane compartments for utilization, feedback metabolism regulation, and storage as cytoplasmic cholesteryl ester lipid droplets (9). Distribution of cholesterol from LE/LYS to other membrane compartments requires NPC1 and NPC2, both of which bind to cholesterol (10–12). These two proteins work in concert (13, 14) to export cholesterol from LE to other membrane organelles. In cells with NPC mutations, build-up of cholesterol and other lipids occurs within LE/LYS, leading to relative deficiency of cholesterol in other membrane compartments, including the plasma membrane (PM) (15, 16), endoplasmic reticulum (ER) (17–20), peroxisomes (21), and *trans*-Golgi network (TGN).

Significance

Niemann-Pick type C disease (NPCD) is an incurable genetic neurological disorder. Cells with NPC mutations fail to export cholesterol from endosomal organelle to multiple other organelles. ACAT1 is an enzyme that converts cholesterol to cholesteryl esters for storage. In mutant NPC cells, cholesterol storage still occurs, although at reduced rate. Here we show that in mutant NPC cells, ACAT1 blockade (A1B) decreases cholesterol storage such that it can be utilized to fulfill cholesterol needs in multiple organelles. In mutant NPC1 mice, *Acat1* gene knockout reduces pathological onset and prolongs the lifespan by 34%. This work identifies ACAT1 as a target to treat NPCD and may help to explain why A1B has been reported to ameliorate preclinical models for Alzheimer's disease.

[1]M.A.R. and C.C.Y.C. contributed equally to this work.

[2]To whom correspondence may be addressed. Email: catherine.chang@dartmouth.edu or ta.yuan.chang@dartmouth.edu.

This abnormal membrane cholesterol distribution causes malfunctions in LE/LYS (22) and other membrane organelles (23). Cholesterol overload in LE/LYS also causes cholesterol to accumulate in the inner membranes of mitochondria (24–27).

In addition to receiving exogenous cholesterol, cells produce cholesterol from de novo biosynthesis. Upon synthesis at the ER, sterols promptly move to the PM via mechanisms independent of NPC1 (28). Cholesterol from both endogenous and exogenous sources traverses among various membrane compartments (29, 30). To prevent overaccumulation of free cholesterol in cells, which would result in cellular toxicity (31), the ATP binding cassette transporter A1 (ABCA1) (32) removes excess cholesterol through a lipid efflux process at the PM. In addition, acyl-coenzyme A:cholesterol acyltransferase 1 (ACAT1) (33) (assigned in GenBank as *SOAT1*, which stands for Sterol O-acyltransferase 1) converts a portion of cellular cholesterol to cholesterol esters for storage. ACAT1 is a membrane protein residing at the ER (34) and at the mitochondrial-associated ER membrane (35).

In mutant NPC cells, the delivery of cholesterol from LE/LYS to the ER is severely hampered; however, a substantial amount of cholesterol can translocate from the PM and other organelles to the ER for esterification in an NPC-independent manner (36–38). Here we hypothesize that in mutant NPC cells, A1B diverts the NPC-independent ACAT1 substrate pool to move to other subcellular membrane compartments to fulfill their needs for cholesterol. To test this hypothesis, we adopted a transgenic mouse model for NPCD ($Npc1^{nmf}$ mouse) (39). This $Npc1^{nmf}$ mouse model carries a single D1005G-$Npc1$ mutation that is comparable to mutations that commonly occur in human $Npc1$ patients. Homozygous $Npc1^{nmf}$ mice begin to die by 90 d after birth and exhibit a phenotype that mimics the late-onset, slowly progressing form of NPCD. In the studies presented here, we bred heterozygous $Npc1^{nmf/+}$ mice with global $Acat1^{-/-}$ ($A1^{-/-}$) mice (40), which also have a C57BL/6 background, to produce $Npc1^{nmf/nmf}:A1^{+/+}$ and $Npc1^{nmf/nmf}:A1^{-/-}$ mice. We then performed paired studies by using sex- and age-matched $Npc1^{nmf/nmf}:$ $A1^{+/+}$ ($Npc1^{nmf}$) and $Npc1^{nmf/nmf}:A1^{-/-}$ mice ($Npc1^{nmf}:A1^{-/-}$). Littermates produced from $Npc1^{+/+}:A1^{+/+}$ mice (WT) and $Npc1^{+/+}:A1^{-/-}$ mice ($A1^{-/-}$) were used as nondiseased controls. In addition, we isolated mouse embryonic fibroblast (MEF) cells from $Npc1^{nmf}$, $Npc1^{nmf}:A1^{-/-}$, WT, and $A1^{-/-}$ mice to perform paired studies in vitro in primary cell culture. To evaluate the relevancy of our findings in the context of human disease, we also monitored the effect of an ACAT1-specific inhibitor K604 on human fibroblast (Hf) cells isolated from several patients with NPCD, and Hf cells isolated from a patient with a related lysosomal storage disease, Niemann-Pick disease type A. The results of these complementary in vivo and in vitro experiments are reported here to demonstrate the potential for A1B as a pathway for NPCD treatment.

Results

Acat1 Gene Deficiency ($A1^{-/-}$) Increases Lifespan and Reduces Weight Loss in $Npc1^{nmf}$ Mice.
To evaluate effects of $A1^{-/-}$ on the lifespan of homozygous $Npc1^{nmf}$ mice, WT, $A1^{-/-}$, $Npc1^{nmf}$, and $Npc1^{nmf}:A1^{-/-}$ mice were fed regular chow diet and their lifespan and weight were observed. The age of death for $Npc1^{nmf}$ mice with or without $A1$ was determined as the point where mice could no longer ingest food or water, as described previously (39). Results (Fig. 1A) show that the median survival for $Npc1^{nmf}$ and $Npc1^{nmf}:A1^{-/-}$ mice was 113 d and 138 d, respectively; the mean survival was 102 d and 137 d, respectively. Thus, $A1^{-/-}$ increases mean lifespan in
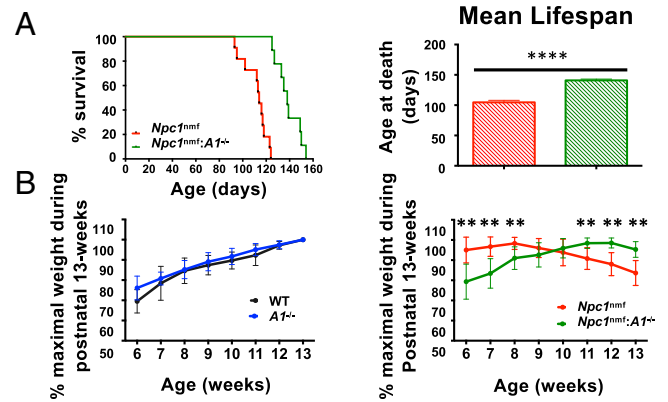

Fig. 1. $A1^{-/-}$ on lifespan and weight loss of $Npc1^{nmf}$ mice. (*A*) $A1^{-/-}$ increases mean lifespan of $Npc1^{nmf}$ mice by 34%. Median survival for $Npc1^{nmf}$ mice and for $Npc1^{nmf}:A1^{-/-}$ mice is 113 d and 138 d, respectively; mean survival is 102 d and 137 d, respectively. $n = 18$ $Npc1^{nmf}$ mice and $n = 16$ $Npc1^{nmf}:A1^{-/-}$ mice. Equal numbers of male and female mice were used. The P value for the log-rank test comparing Kaplan–Meier survival curves is ****$P < 0.0001$. The procedure described in Maue et al. (39) was adopted to define death of the $Npc1^{nmf}$ mouse. (*B*) $A1^{-/-}$ delays the weight loss of $Npc1^{nmf}$ mice (*Right*) without affecting the weight of WT mice (*Left*). Weight measurement began at 6 wk of age. Data are expressed as percent of maximum weight during the first 13 wk. $n = 10$ mice per group. Error bars indicate 1 SEM. For the *Right*, except for weeks 9 ($P = 0.2$) and 10 ($P = 0.4$), the P value for weight in each week, comparing $Npc1^{nmf}:A1^{-/-}$ vs. $Npc1^{nmf}$, is **$P < 0.003$. For the *Left*, there are no significant differences in weight in each week for WT vs. $A1^{-/-}$.

$Npc1^{nmf}$ mutant mice by 34%. In control experiments, no spontaneous deaths occurred in either WT or $A1^{-/-}$ mice up to 17 mo of age. We next evaluated the effect of $A1$ gene alteration on the total body weight of $Npc1^{nmf}$ mice starting at 6 wk of age. Results (Fig. 1 *B*, *Right*) show that $Npc1^{nmf}$ mice began to lose weight ~9 wk of age. In contrast, mutant mice also lacking the $A1$ gene did not begin to lose weight until 13 wk of age. Thus, $A1^{-/-}$ delayed the onset of weight loss observed in $Npc1^{nmf}$ mice. In control experiments (Fig. 1 *B*, *Left*) $A1^{-/-}$ mice weighed slightly less than WT mice at 6 wk of age, but this difference disappeared at 8 wk and older.

$A1^{-/-}$ Reduces Cellular Pathology in Liver, Spleen and Cerebellum in $Npc1^{nmf}$ Mice.
NPCD exhibits accumulation of large foamy macrophages in various tissues. To determine if A1B has any effect on foam cell pathology in $Npc1^{nmf}$ mice, we isolated tissues from mice of four genotypes at postnatal day 80 (P80) and performed histological analyses. When compared with $Npc1^{nmf}$ mice, $Npc1^{nmf}:A1^{-/-}$ mice had markedly reduced foam cell pathology in the liver (Fig. 2 *A*, *Right*: *Upper* vs. *Lower*) and the spleen (Fig. 2 *B*, *Right*: *Upper* vs. *Lower*). In the lung, however, foam cell pathology in these two genotypes was comparable (Fig. 2 *C*, *Right*: *Upper* vs. *Lower*). The control experiments confirmed that neither WT nor $A1^{-/-}$ mice exhibit appreciable foam cell pathology in any of these three tissues (Fig. 2 *A–C*, *Left*: *Upper* vs. *Lower*). Previous studies in mutant NPC animals have demonstrated that extensive Purkinje neuron death occurs in the cerebellum prior to the death of the animals. To evaluate the effect of $A1^{-/-}$ on $Npc1^{nmf}$ Purkinje neurons, the cerebellum was isolated from P80 mice and the numbers of Purkinje neurons were counted after histochemical staining of thin slices. As shown (Fig. 2D), when compared with WT mice and in $A1^{-/-}$ mice, $Npc1^{nmf}$ mice had fewer than 20% residual Purkinje cells, whereas $Npc1^{nmf}:A1^{-/-}$ mice had more than 30% residual Purkinje cells (Fig. 2 *D*, *Right* two panels). These results demonstrate that in
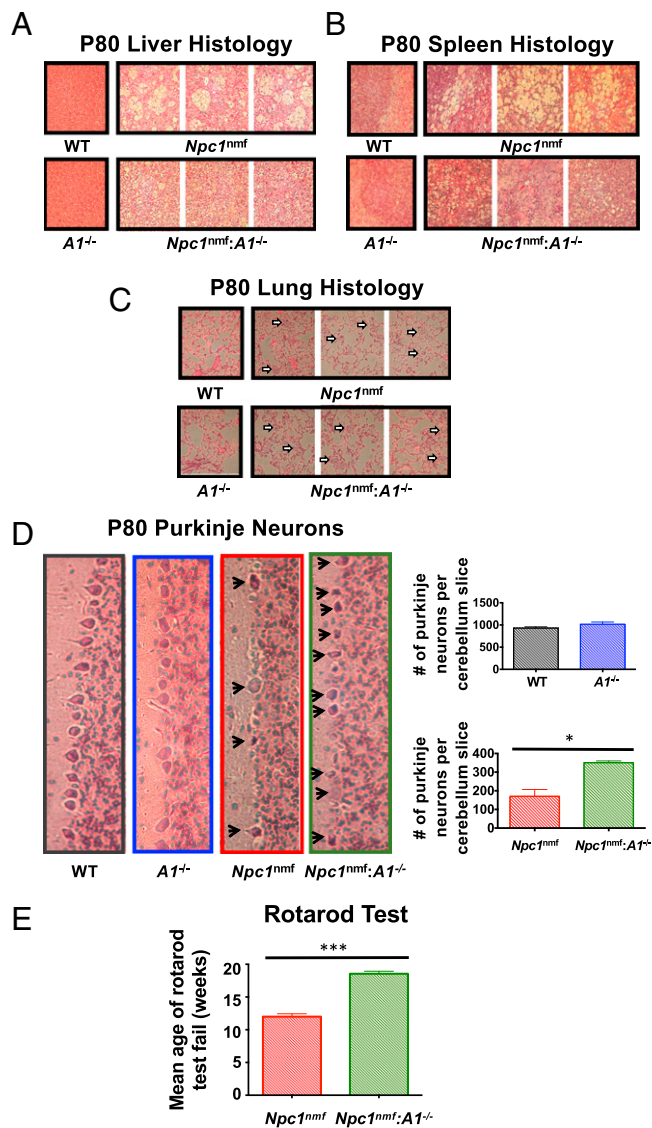
Fig. 2. Effects of $A1^{-/-}$ on cellular pathology, neuronal loss, and motor deficits in $Npc1^{nmf}$ mice. (*A–C*) $A1^{-/-}$ improves macrophage foam cell pathology in liver (*A*), and spleen (*B*), but not in lung (*C*) of the $Npc1^{nmf}$ mouse. Tissues were isolated from mice at P80, fixed, and cut into thin slices for H&E staining. Images are at 40×. Results are representative from three mice per group. For *C*, arrows point at foam cells. (*D*) $A1^{-/-}$ partially prevents Purkinje neuron death in $Npc1^{nmf}$ mice, without affecting Purkinje neuron numbers in WT mice; 10× magnification of representative images of the cerebellum in the WT, $A1^{-/-}$, $Npc1^{nmf}$, and $Npc1^{nmf}$: $A1^{-/-}$ mice, highlighting the relative number of Purkinje neurons. The relative numbers of Purkinje neurons (indicated by arrows in the images, *Right*) were quantitated by counting in two separate lobes; $n = 6$ animals per group. (*Right Lower*) Comparison of number of Purkinje neurons between $Npc1^{nmf}$:$A1^{-/-}$ and $Npc1^{nmf}$. Error bars indicate 1 SEM. (*E*) $A1^{-/-}$ improves motor performance in $Npc1^{nmf}$ mice. The motor performance test was as described in *SI Appendix, Materials and Methods*. $n = 13$ $Npc1^{nmf}$ mice and $n = 11$ $Npc1^{nmf}$: $A1^{-/-}$ mice. Comparable numbers of males and females were employed. The *P* value is for mean age at failure of motor performance test, comparing $Npc1^{nmf}$:$A1^{-/-}$ and $Npc1^{nmf}$. *$P = 0.0173$; ***$P < 0.001$.

the $Npc1^{nmf}$ mouse model, $A1$ gene ablation significantly decreases the loss of Purkinje neurons in the brain.

$A1^{-/-}$ Ameliorates Motor Deficits in $Npc1^{nmf}$ Mice. Mutant $Npc1^{nmf}$ mice exhibit a decline in motor performance, beginning at ~11 wk of age. We monitored the motor performance of WT, $A1^{-/-}$, $Npc1^{nmf}$, and $Npc1^{nmf}$:$A1^{-/-}$ mice beginning at 9 wk of age by using a rotarod test, which tests sensorimotor coordination and balance. Among $Npc1^{nmf}$ mice, the mean age

of failing or not running on the rotarod test occurred at ~12 wk of age, whereas among $Npc1^{nmf}$:$A1^{-/-}$ mice, the mean age of failure occurred at 18 wk of age (Fig. 2*E*). Control experiments showed that at the same age, neither WT nor $A1^{-/-}$ mice failed the rotarod test. These results demonstrate that $A1$ gene ablation delays the loss of sensorimotor coordination and balance in $Npc1^{nmf}$ mice.

Cholesterol Analysis in Mouse Brain, and MEF: Content, Esterification, and Distribution. To determine whether $A1^{-/-}$ alters total free cholesterol content in the $Npc1^{nmf}$ mouse brain, we isolated whole brains from mice of four genotypes at P90 and measured their total free (unesterified) cholesterol content. We found comparable cholesterol content across these samples (Fig. 3*A*). We next isolated MEFs from these mice, grew them in DMEM with 10% serum in monolayers until confluency, and then harvested the cells for analysis of total free cholesterol content. The results (Fig. 3*B*) show that the free cholesterol content in these four cell types was also similar.

We next measured relative cholesterol ester biosynthesis rates in these cells by feeding them with labeled ^{3}H-oleate for 20 min and then measuring production of ^{3}H-cholesteryl oleate. The results (Fig. 3 *C* and *D*, columns 1 to 4) show that when grown in lipoprotein-containing medium, WT cells exhibited an ample cholesterol ester biosynthesis rate. As expected, in cells without ACAT1 (i.e., $A1^{-/-}$ and $Npc1^{nmf}$:$A1^{-/-}$ cells), the cholesterol ester biosynthesis rate was only 2% that of WT cells. In $NpC1^{nmf}$ cells, *the* rate was ~34% of WT cells. When these four cell types were grown in 10% delipidated serum medium (i.e., medium devoid of most exogenous cholesterol), the cholesteryl ester biosynthesis rate decreased drastically in WT cells, and also decreased in the other three cell types (Fig. 3*D*, columns 5 to 8). When low-density lipoproteins (LDL) were added to the delipidated serum medium for 3 or 6 h, however, the cholesteryl ester biosynthesis rate was restored in WT cells in a time-dependent manner. Adding LDL also increased the cholesteryl ester biosynthesis rate in mutant $Npc1^{nmf}$ cells, but not nearly to the level observed in WT cells (Fig. 3*D*, comparing red bars vs. black bars). These results show that within a 3- to 6-h period, mutant $Npc1^{nmf}$ cells fail to utilize LDL-derived cholesterol efficiently for esterification. As expected, in $A1^{-/-}$ and $Npc1^{nmf}$:$A1^{-/-}$ cells, within the 3- to 6-h time frame, the LDL-dependent increase in cholesterol ester biosynthesis rate was abolished (Fig. 3*D*, comparing blue and green bars vs. black bars). The results presented in Fig. 3 *C* and *D*, columns 1 to 4 show that when maintained in the lipoprotein-containing medium at a steady state, $Npc1^{nmf}$ cells exhibit a residual cholesterol ester biosynthesis of ~34% compared with WT cells. Thus, in addition to using cholesterol derived from the NPC-containing LEs for esterification, cells can also use cholesterol sources independent of NPC1 for esterification at the ER.

Cholesterol Distribution in Subcellular Organelles of MEF Cell Homogenates. Because ACAT1 plays a key role in cholesterol storage, we postulate that $A1^{-/-}$ in both WT and $Npc1^{nmf}$ MEF may cause substantial alterations in cellular cholesterol distribution among various membrane organelles. To test this possibility, we first performed intact cell staining with filipin, a small, natural fluorescent molecule that binds to cholesterol, and then viewed cells using confocal fluorescent microscopy. The results are shown in *SI Appendix,* Fig. S1. To use a separate, biochemical approach to examine the membrane cholesterol distribution in these four cell types, we performed
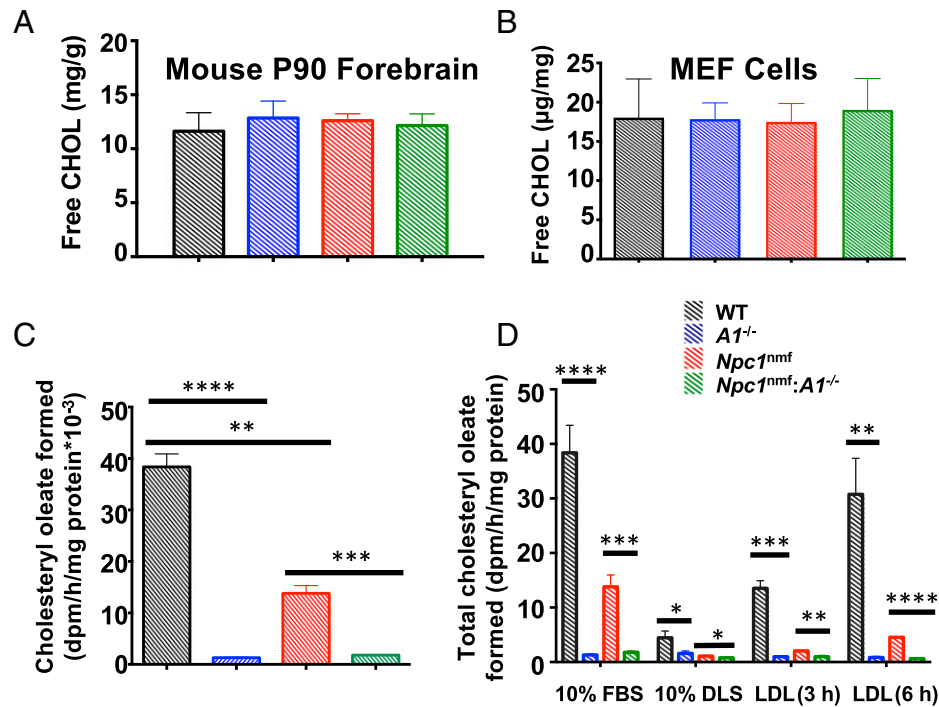
Fig. 3. Cholesterol content in mouse brain (A) and MEFs (B); cholesteryl ester biosynthesis in MEFs grown continuously in lipoprotein-containing medium (C) or in delipidated serum medium in response to LDL (D). (A) Free cholesterol content in P90 mouse forebrain. Procedure is described in *SI Appendix, Materials and Methods*; *n* = 5 mice (3 male and 2 female) per group. Error bars indicate 1 SEM. (B) Free cholesterol content in MEFs. Three individual clones per genotype were employed. Cells were seeded in six-well plates at 200,000 cells per well and grown in DMEM plus 10% serum to near confluence. After three washes with PBS, cells were scraped as suspensions in PBS and used for protein measurement, and lipid extraction by chloroform/methanol. Cholesterol content was determined as described in *SI Appendix, Materials and Methods*. (C) Cholesteryl ester biosynthesis in MEFs continuously grown in lipoprotein-containing medium. Three individual clones per cell type were used. Cells were grown as described in *B*. Cholesteryl ester synthesis in intact cells was conducted as described in Chang et al. (68). (D) Cholesterol ester biosynthesis in MEFs grown in cholesterol-containing medium (10% FBS), cholesterol-free medium (10% DLS), or 10% DLS in response to LDL feeding for 3 h or 6 h. Cholesteryl ester biosynthesis in intact cells was conducted as described in Chang et al. (68).

subcellular fractionation of postnuclear cell homogenates prepared from the MEFs, using OptiPrep density gradient ultracentrifugation. This method produces partial separation of various membrane organelles, based primarily on their buoyant densities. After OptiPrep fractionation, we analyzed the distribution of various membrane organelles in these fractions by performing Western blot analyses of protein markers for LE/LYS (LAMP1), TGN (syntaxin 6), *cis*-Golgi (GM130), PM (caveolin 1), ER (calnexin), and mitochondria (cytochrome C oxidase) (Fig. 4*A*). We also analyzed cholesterol content in each fraction (Fig. 4*B*). Western analyses (Fig. 4*A*) show that in all four cell types, LE/LYS (LAMP1$^+$) signals were tightly enriched in fractions #1 to #3 (with light density), and mitochondria (cytochrome-C-oxidase$^+$) signals were tightly enriched in fractions #9 to #11 (with heavy density). Mutant *Npc1*^{nmf} cells, but not *Npc1*^{nmf}:*A1*$^{-/-}$ cells, exhibited additional LE/LYS signals with heavier density in fractions #5 to #9. The distributions of TGN and *cis*-Golgi signals were comparable among the four cell types, but in mutant *Npc1*^{nmf} cells both of these signals exhibited a broader range in density. ER signals in all four cell types were comparable. PM signals were enriched in fractions #5 to #8 in WT cells, but shifted to slightly later fractions (#7 to #9) in *A1*$^{-/-}$ cells. In mutant *Npc1*^{nmf} cells and in *Npc1*^{nmf}:*A1*$^{-/-}$ cells, PM signals were enriched in fractions #5 to #8, with the PM in *Npc1*^{nmf}:*A1*$^{-/-}$ cells exhibiting a broader range in density. These results show that except for the abnormal LE/LYS signals in mutant *Npc1*^{nmf} cells, the buoyant densities of LE/LYS, *cis*-Golgi, TGN, mitochondria, ER, and PMs in these four cell types are comparable, with the TGN and *cis*-Golgi signals in mutant *Npc1*^{nmf} cells exhibiting a broader range in density.

Cholesterol content analyses in the OptiPrep fractions (Fig. 4*B*) show that in WT cells, as expected, cholesterol was highly enriched in the PM fraction (#5 to #8), whereas membranes with slightly heavier densities, including the ER membranes (#7 to #9) and the mitochondrial membranes (#9 to #11), had much less cholesterol content. In contrast, in *A1*$^{-/-}$ cells the membranes with heavier densities, including the ER and mitochondria, were enriched in cholesterol. In mutant *Npc1*^{nmf} cells, cholesterol was highly enriched in the light-density LE/LYS (fractions #1 to #3). By comparison, in *Npc1*^{nmf}:*A1*$^{-/-}$ cells, the cholesterol contents of LE/LYS were significantly diminished, whereas the cholesterol contents in the Golgi-like membranes (#2 to #6), PM-like membranes (#5 to #8), and ER-and mitochondria-like membranes (#7 to #11) were all relatively enriched. These results, along with results presented in *SI Appendix*, Fig. S1, suggest that in *Npc1*^{nmf} cells, cholesterol is mostly sequestered within LE/LYS; deletion of the *A1* gene in *Npc1*^{nmf}:*A1*$^{-/-}$ cells causes major changes in cholesterol distribution in various membrane organelles.

Relative Alkyne Cholesterol Distribution in Various Subcellular Compartments of Intact MEFs. The results described in Fig. 4*B* suggested that *A1*$^{-/-}$ in *Npc1*^{nmf} cells causes cholesterol content in LE/LYS to decrease, while it causes cholesterol content to increase in various other membrane organelles, including the Golgi, PM, ER, and mitochondria. Since the OptiPrep fractionation procedure provides incomplete separation among membrane organelles, we used an additional method to validate these results. Various analogs of lipids containing an alkyne moiety can react rapidly to azides (41, 42) and produce covalent adducts after conducting click chemistry (43). When the
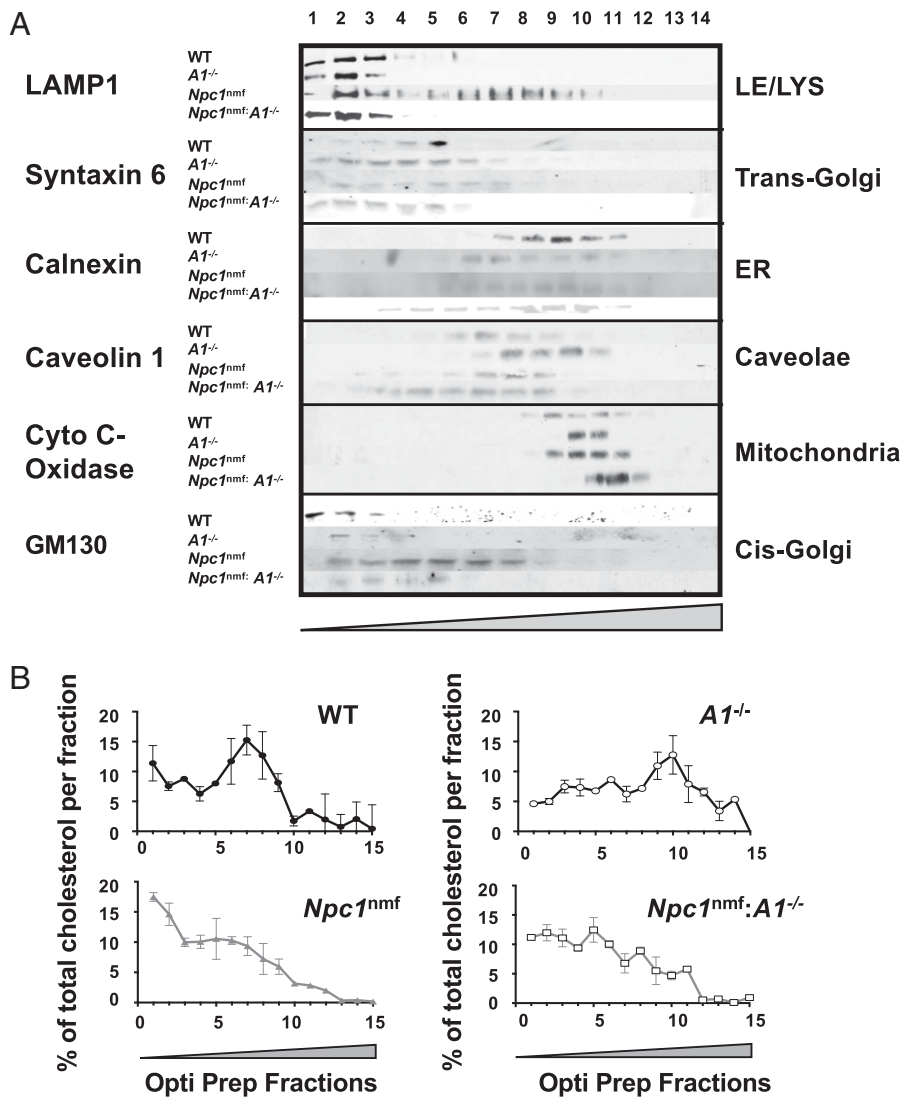
Fig. 4. Cellular cholesterol distribution in MEFs. (*A*) Localization of subcellular organelles after cell fractionation. Procedure for subcellular fraction is described in *SI Appendix, Materials and Methods*. Antibodies for specific protein markers (listed on far left) were used to localize specific organelles (listed on right). (*B*) Cholesterol distribution in various subcellular organelles. Procedure for cholesterol analysis is described in *SI Appendix, Materials and Methods*. The values reported were normalized by total cholesterol content present in all fractions. Data are means ± 1 SD from two separate experiments. Gray arrows at bottom indicate gradual changes in density from light (fraction 1) to heavy (fraction 14).

azides are tagged with a fluorescent probe, these lipid analogs become highly fluorescent. This strategy has been utilized to report the subcellular localization and metabolism of natural lipids in intact cells. As a reagent for detecting cholesterol, the sensitivity of the alkyne analog of cholesterol, 27-alkyne cholesterol [(25 R)-25-ethinyl-26-no-3 β-hydroxy cholest-5-en] (44), is far superior to filipin. When fed to cells, 27-alkyne cholesterol is clearly detectable in various membrane organelles, including the ER, LE/LYS, TGN, and mitochondria (44). Here we first labeled mutant $Npc1^{nmf}$ and $Npc1^{nmf}:A1^{-/-}$ MEFs by transient transfections with one of the fluorescent markers for the ER, LE/LYS, TGN, and mitochondria, then grew these cells in serum-containing medium, and fed them with 27-alkyne cholesterol at a very low concentration (0.5 μM) for 18 h. To serve as controls, in the last 90 min some of the mutant $Npc1^{nmf}$ cells were also fed with 30 μg/mL (77 μM) of cholesterol. Cells were subject to click chemistry reaction with a fluorescent azide, followed by fluorescent confocal microscopy to monitor the fluorescence intensity of 27-alkyne cholesterol associated with the individual organelle markers. To minimize the difference in expression levels of the organelle cell markers, 12 to 32 individual cells were viewed. The average values were used to compare the relative amount of 27-alkyne cholesterol associated with each organelle in mutant $Npc1^{nmf}$ and $Npc1^{nmf}:A1^{-/-}$ MEFs.

Results showed that in mutant $Npc1^{nmf}$ MEFs, $A1^{-/-}$ significantly decreased the 27-alkyne cholesterol contents associated with LE/LYS (with GFP-LAMP1 as the marker) (Fig. 5*A*). $A1^{-/-}$ also significantly increased 27-alkyne cholesterol contents associated with TGN-rich membrane (with GFP-syntaxin 6 as the marker) (Fig. 5*B*), and those associated with mitochondria (with BFP-cytochrome C oxidase as the marker) (Fig. 5*C*). $A1^{-/-}$ did not significantly alter the 27-alkyne cholesterol associated with the ER (with BFP-KDEL sequence as the marker) (Fig. 5*D*). These results largely corroborate with the results obtained by using Optiprep fractionation (Fig. 4). An important difference is that the image analyses provide a method to distinguish 27-alkyne cholesterol associated with mitochondria versus that associated with the ER, while the Optiprep fractionation method was unable to provide clean separation between
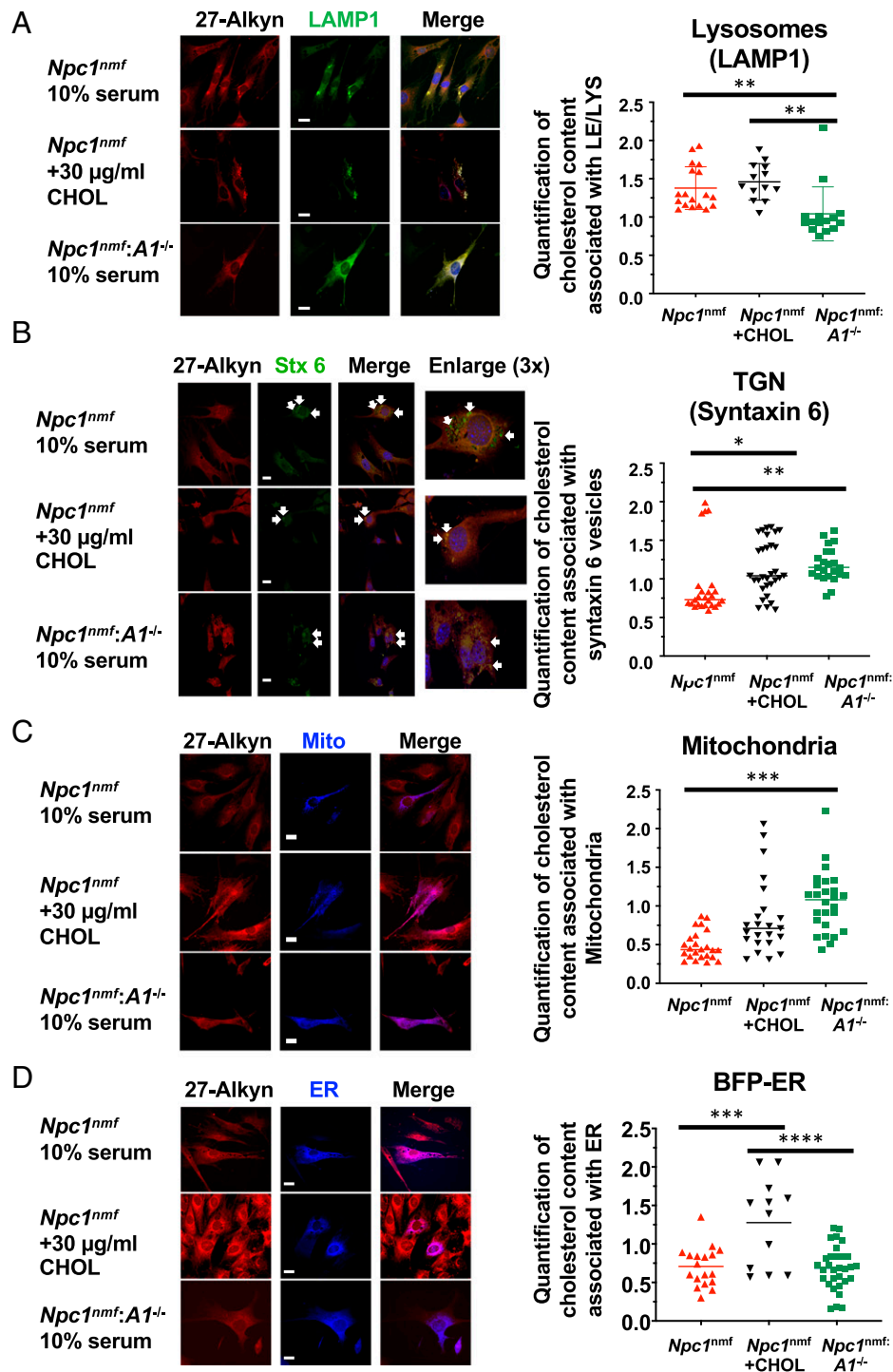
Fig. 5. Distribution of alkyne cholesterol in various subcellular compartments of *Npc1^nmf* and *Npc1^nmf:A1^−/−* MEFs. MEF cells were seeded in six-well plates containing 10% serum. When cell density reached ∼80% confluence, cells were transiently transfected with FP-tagged markers, as indicated (*A–D*). When cells became confluent, they were trypsinized and seeded on glass coverslips pretreated with poly-D-lysine; 27-alkye cholesterol were added to growth media at 0.5-µM final concentration for around 18 h. Cells were then rinsed and fixed with 4% paraformaldehyde, followed by click chemistry with 1 µM Alexa 594-azide, incubated for 30 min in the dark, then processed as described in *SI Appendix, Materials and Methods*. (Scale bars, 25 µm.) (*A*) Representative images of alkyne cholesterol (red) and LAMP1-Emerald as the LE/LYS marker; and the quantification of cholesterol content associated with LE/LYS, as described in *SI Appendix, Materials and Methods*. (*B*) Representative images of alkyne cholesterol (red) and GFP-syntaxin 6 as TGN marker, and the quantification of cholesterol content associated with TGN. Arrows highlight the syntaxin 6-positive vesicles. (*C*) Representative images of alkyne cholesterol (red) and Mito-BFP (blue) as the mitochondria marker; and the quantification of cholesterol content associated with mitochondria. (*D*) Representative images of alkyne cholesterol (red) and BFP-ER (blue) as the ER marker; and the quantification of cholesterol content associated with the ER. *$P < 0.05$; **$P < 0.01$; ***$P < 0.001$; ****$P < 0.0001$.

the ER and mitochondria. The results of the control experiment showed that delivering cholesterol exogenously to mutant *Npc1^nmf* cells (for 90 min) also increased 27-alkyne cholesterol contents in TGN-rich membranes (Fig. 5*B*), as well as in mitochondria (Fig. 5*C*). However, unlike the effects of *A1^−/−*, delivering cholesterol exogenously increased the 27-alkyne cholesterol contents at the ER (Fig. 5*D, Left*, second row), but did not alter the 27-alkyne cholesterol contents in LE/LYS (Fig. 5*A*). These results show that exogenous cholesterol affects membrane cholesterol distribution in a manner differently than A1B.

$A1^{-/-}$ Ameliorates the Mislocalization of Syntaxin 6 and Golgin 97 in Intact Mutant $Npc1^{nmf}$ MEFs. Syntaxin 6 binds to cholesterol (45) and is one of the t-SNARE proteins in vesicles that participate in various membrane fusion events. In normal cells, most of the syntaxin 6 signal is found at the TGN (46), which is rich in cholesterol content (47), and plays a key role in transporting proteins and lipids to other membrane compartments. In mutant NPC cells, TGN fails to receive LDL-derived cholesterol from LEs (48). This deficiency causes syntaxin 6 to be mislocalized from the TGN and exhibit an abnormal, scattered cytoplasmic pattern. Treating mutant NPC1 cells with cholesterol/cyclodextrin complex, or a high concentration of LDL for 24 h, restores syntaxin 6 to the one-sided, perinuclear Golgi localization pattern observed in normal cells. Several other t-SNARE proteins tested do not show cholesterol-sensitive localization patterns (23). Based on these findings, as well as results presented in Fig. 4 and *SI Appendix*, Fig. S1, we postulated that $A1^{-/-}$ may correct the mislocalization pattern of syntaxin 6 observed in mutant $Npc1^{nmf}$ MEFs. To test this possibility, we performed immunofluorescence confocal microscopy in fixed, intact cells using antibodies specific for syntaxin 6. The results (Fig. 6A) show that in WT cells and in $A1^{-/-}$ cells, most of the syntaxin 6 signals were highly polarized to only one side of the space adjacent to the nucleus, exhibiting a typical Golgi distribution pattern typical of mammalian cells. In contrast, in mutant $Npc1^{nmf}$ cells (Fig. 6 A, third row), a large portion of the syntaxin 6 signal was distributed in scattered cytoplasmic vesicular structures around both sides of the nucleus. These results support earlier findings (23) demonstrating that a sizable portion of syntaxin 6$^+$ signals become adjacent to or part of the recycling endosomes. In contrast, $Npc1^{nmf}:A1^{-/-}$ cells (Fig. 6A, fourth row) expressed the normal syntaxin 6 distribution patterns (i.e., the one-sided, perinuclear pattern observed in WT and $A1^{-/-}$ cells).

To quantitate the difference in the syntaxin 6 distribution pattern observed in the MEFs of the four genotypes, we measured the "reflex angle," defined as the angle subtended by the edges of the syntaxin 6$^+$ signals, using the center of the nucleus (DAPI$^+$ signal) as the vertex (49). The results (Fig. 6 A, *Right*) show that for WT and $A1^{-/-}$ cells, the reflex angles were similar at 121° and 115°, respectively. For mutant $Npc1^{nmf}$ cells, the reflex angle was much larger at 280°, whereas it was largely restored to 120° for $Npc1^{nmf}:A1^{-/-}$ cells. Control experiments (Fig. 6B) showed that the normalized syntaxin 6 protein content in all four cell types was comparable. Together, these results show that $A1^{-/-}$ largely rectifies the mislocalization of syntaxin 6 observed in mutant $Npc1^{nmf}$ cells, without affecting its protein content.

To strengthen these results, we sought to examine the localization pattern of a second protein marker of the TGN. Golgins are peripheral membrane proteins located mainly at the membrane surface of TGN (50). In humans there are four golgins, each playing a distinct role in membrane protein transport events. Using antibodies specific for golgin 97 (GCC97), we performed double-immunofluorescence experiments to compare the localization patterns of syntaxin 6 (red signal) and golgin 97 (green signal) in the four MEF cell types. In WT cells (Fig. 6C, first row, second column), the golgin 97 signal exhibited a typical polarized Golgi distribution pattern. In $A1^{-/-}$ cells (Fig. 6C, second row, second column), most of the golgin 97 signals exhibited a pattern similar to that in WT cells, with a minority of the golgin 97 signal appearing as part of small, punctate structures, perhaps corresponding to internal membrane organelles. In $Npc1^{nmf}$ cells (Fig. 6C, third row, second

column), the golgin 97 signals was dispersed and scattered within the space around the nucleus, and a pattern is clearly distinct from that observed in WT cells and $A1^{-/-}$ cells. In contrast, in $Npc1^{nmf}:A1^{-/-}$ cells (Fig. 6C, fourth row, second column), the abnormal golgin 97 mislocalization in $Npc1^{nmf}$ cells was largely corrected. For clarity, the last column of Fig. 6C provides 6× enlarged images.

We next performed double-immunofluorescence experiments and monitored the degree of apparent colocalization between syntaxin 6 (red signal) and golgin 97 (green signal) in the four cell types (Fig. 6C). As shown, in WT and $A1^{-/-}$ cells, the apparent colocalization between syntaxin 6 and golgin 97 was relatively low (21 to 32%). Mutation in NPC1 caused the colocalization index to increase to 51%, while $Npc1^{nmf}:A1^{-/-}$ cells reduced the colocalization index back to 24%, a value comparable to that in WT and $A1^{-/-}$ cells. Consistent with previous studies, these results show that under normal conditions, most of the syntaxin 6 and Golgi 97 are located in different domains of TGN (51). In mutant NPC cells, a substantially large fraction of these proteins became colocalized.

To serve as a control, we next examined the localization pattern of GM130, the protein marker for *cis*-Golgi, in MEFs of the four genotypes. These results (Fig. 6D) support a previous finding that in mutant NPC-like cells, GM130 was more concentrated (51). Our results are also consistent with the previous report that in mutant NPC1 cells, the morphology of the Golgi apparatus viewed under electron microscopy remains largely unaltered (23). By reflex angle measurement, however, we found that GM130 protein was more condensed on one side of the nucleus (126°) in $Npc1^{nmf}$ cells (Fig. 6D, third row) than in WT cells (174°) or in $A1^{-/-}$ cells (201°), whereas in $NPC1^{nmf}:A1^{-/-}$ cells (Fig. 6D, fourth row) GM130 localization was corrected back to a more even distribution (178°). Together, these results suggest that NPC mutation affects the morphology of certain microdomains of the TGN that are enriched in syntaxin 6 and golgin 97, potentially leading to subtle, secondary morphological changes in the rest of the Golgi apparatus; these abnormalities can all be corrected by A1B.

$A1^{-/-}$ Restores Diminished Levels of Cation-Dependent Mannose-6-Phosphate Receptor and Cathepsin D Protein Contents in Mutant $Npc1^{nmf}$ MEFs. Syntaxin 6 at TGN is involved in the anterograde vesicular trafficking of mannose-6-phosphate receptors (M6PRs)/lysosomal hydrolase complexes (46). The cation-dependent (CD) and cation-independent (CI) mannose-6-phosphate receptors (CD-M6PR and CI-M6PR) deliver newly synthesized lysosomal enzymes from the TGN to LEs; M6PRs then recycle back to the TGN for reutilization (52). In mutant NPC cells, the CD-M6PR localization pattern is altered from residing mostly at the TGN to residing mostly in the cholesterol-laden LEs (53). Furthermore, in mutant NPC cells, cholesterol accumulation causes CD-M6PR to be rapidly degraded in LE/LYS (54). Since we found that $A1^{-/-}$ rescued syntaxin 6 and golgin 97 from mislocalization in mutant $Npc1^{nmf}$ cells (Fig. 6A), we hypothesized that $A1^{-/-}$ may also affect M6PR protein expression in mutant $Npc1^{nmf}$ cells. To test this possibility, we performed Western blot analyses to monitor the levels of CD-M6PR protein in the four different MEFS. Compared with WT cells, $Npc1^{nmf}$ cells expressed CD-M6PR at levels less than 20% of values in WT cells (Fig. 7A). In contrast, $Npc1^{nmf}:A1^{-/-}$ cells expressed CD-M6PR at levels more than double those of WT cells. These findings suggest that $A1^{-/-}$ more than compensated for the low protein expression of the CD-M6PR in $Npc1^{nmf}$ cells, We
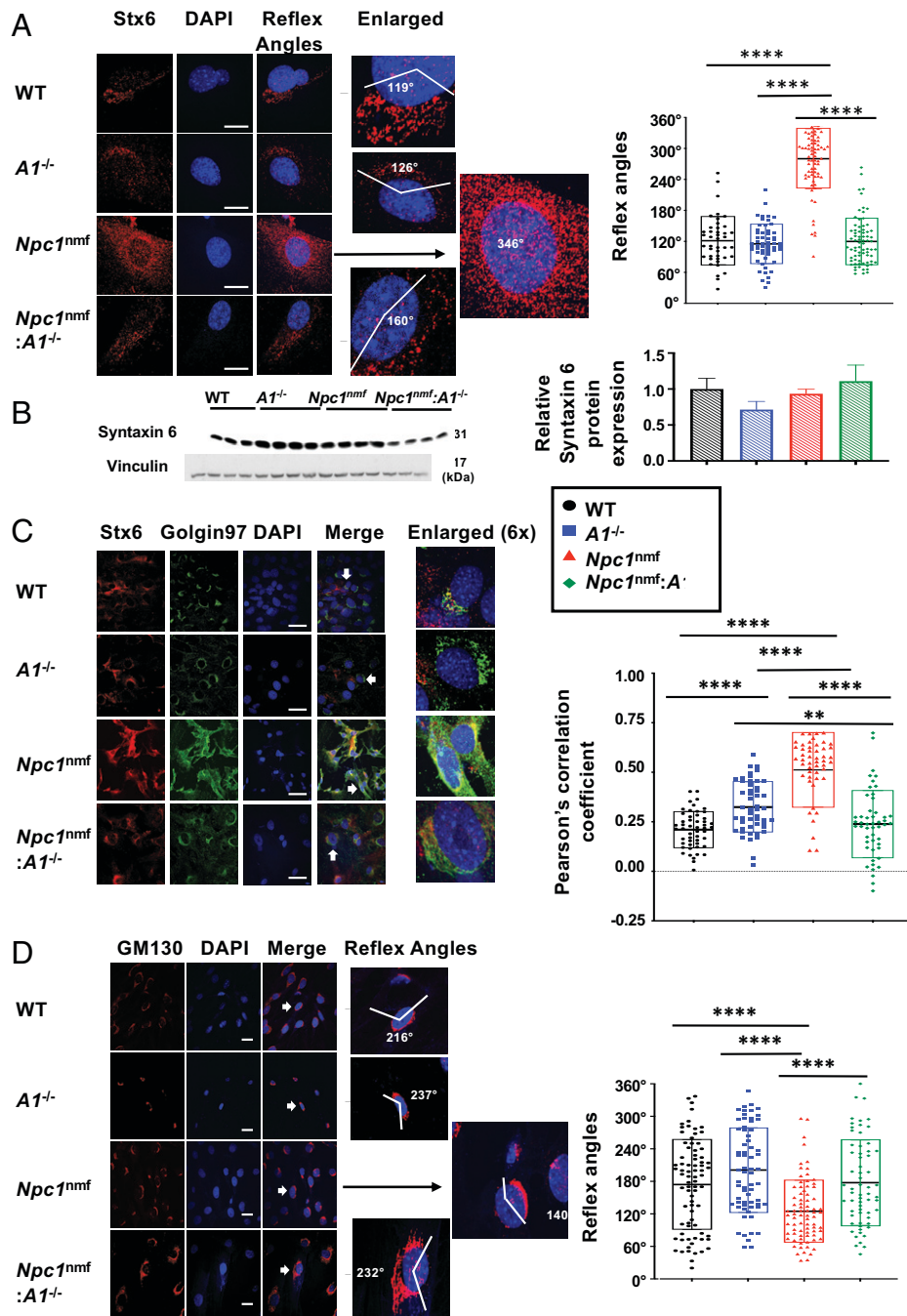
Fig. 6. Immunofluorescent staining and Western blots of MEFs. (*A*) Syntaxin 6 localization and reflex angles measurement in fixed intact MEFs, and the quantification of the reflex angles. Cells were seeded and processed as described in *SI Appendix, Materials and Methods*. (Scale bars, 25 μm.) (*B*) Relative protein contents of syntaxin 6 in MEFs. Cells were seeded and processed as described in *SI Appendix, Materials and Methods*. Two-hundred microliters of 10% SDS was added per dish, and 150 μg of the solubilized protein was loaded per lane for Western analyses using antisyntaxin 6 antibodies. Protein levels were normalized by using vinculin as the loading control. Error bars indicate 1 SEM. (*C*) Double immunofluorescence of syntaxin 6 and golgin 97, and degree of apparent colocalization between syntaxin 6 and golgin 97 in fixed intact MEFs. Cells were seeded and processed as described in *SI Appendix, Materials and Methods*. (Scale bars, 20 μm.) (*D*) GM130 localization and reflex angles measurement in intact MEFs. Procedures for confocal microscopy viewing, reflex measurement, and calculation of apparent colocalization calculations are described in *SI Appendix, Materials and Methods*. (Scale bars, 25 μm.) **$P < 0.01$; ****$P < 0.0001$.

also found that $A1^{-/-}$ cells expressed CD-M6PR at 50% of values found in WT cells; the basis for $A1^{-/-}$ decrease CD-M6PR level in WT cells is unclear.

Cathepsin D is one of the major lysosomal enzymes that requires M6PRs for processing at the TGN. From the TGN, the cathepsin D/M6PRs complexes move to LE/LYS for maturation by proteolysis. Cathepsin D exists in various forms, including precursor, intermediate, and proteolytically cleaved mature heavy chain and light chain. These forms exhibit different molecular weights on SDS/PAGE (55). In light of our

finding that CD-M6PR expression is very low in mutant $NPC1^{nmf}$ cells, and that $A1^{-/-}$ rescued this deficiency (Fig. 7*B*), we postulated that mutant $NPC1^{nmf}$ MEFs may express a lower level of cathepsin D protein (the mature heavy chain), and that $A1^{-/-}$ may correct this abnormality. To test this possibility, we performed Western blot analyses by using a highly specific monoclonal antibody against the cathepsin D mature heavy chain. We found that in WT and $A1^{-/-}$ MEF cells, this antibody recognized the mature form of cathepsin D heavy chain, which has an apparent size of 30 to 32 kDa (Fig. 7*B*).
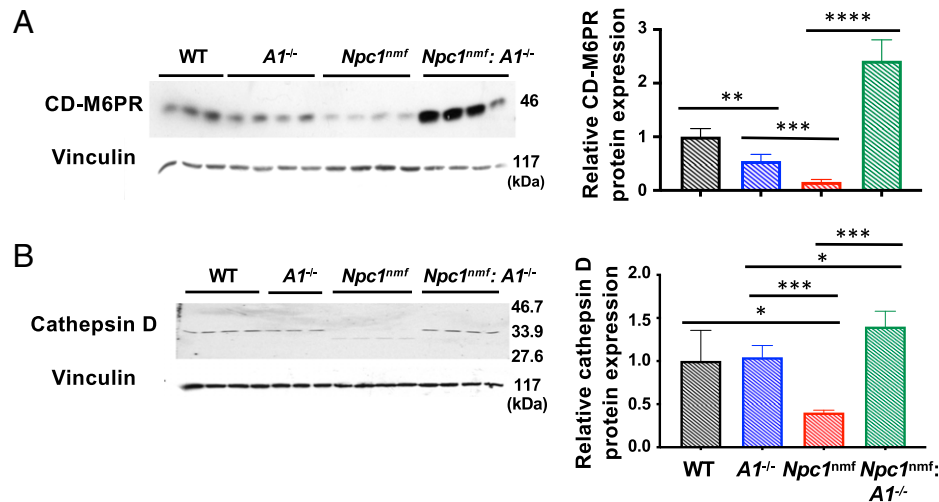
Fig. 7. Relative protein content and gene expressions in MEFs and mouse cerebellum. (*A*) Relative protein content of CD-M6PR (46 kDa) in MEFs. Cells were seeded and processed as described in *SI Appendix, Materials and Methods*. (*B*) Relative protein content of cathepsin D (mature form heavy chain) (30 to 32 kDa in WT, $A1^{-/-}$, and $Npc1^{nmf}:A1^{-/-}$ cells; 28 kDa in $Npc1^{nmf}$ cells). Cells were seeded and processed as described in *SI Appendix, Materials and Methods*. *$P < 0.05$; **$P < 0.01$; ***$P < 0.001$; ****$P < 0.0001$.

Furthermore, WT and $A1^{-/-}$ cells expressed this mature form at comparable levels, whereas expression in mutant $Npc1^{nmf}$ cells was 64% lower. In addition, the mature form of cathepsin D present in $NPC1^{nmf}$ cells was slightly smaller (by 2 to 3 kDa) than that found in WT and $A1^{-/-}$ cells, suggesting that abnormal proteolytic cleavage of cathepsin D might occur within the LE/LYS of $NPC1^{nmf}$ cells. In contrast, $Npc1^{nmf}:A1^{-/-}$ expressed cathepsin D at the same size as found in WT and $A1^{-/-}$ cells, with protein levels 40% higher than those found in WT and $A1^{-/-}$ cells. Together, these results show that in $Npc1^{nmf}$ cells, $A1^{-/-}$ reversed the diminished levels of CD-M6PR and cathepsin D protein expression, consistent with both of these proteins being downstream targets of syntaxin 6-mediated vesicular trafficking.

A1B Increased ABCA1 Protein Levels in *Npc1^{nmf}* MEFs and in *Npc1^{nmf}* Mouse Cerebellum. The results described above show that in $Npc1^{nmf}$ cells, cathepsin D protein content is significantly decreased and can be restored by $A1^{-/-}$. To substantiate this finding, we sought to examine a relevant downstream target of cathepsin D-mediated signaling. We focused on ABCA1, which functions as a key cellular cholesterol efflux protein (56). ABCA1 is transcriptionally regulated by liver X receptors (57, 58) and posttranslationally regulated by various degradation mechanisms (59). In mutant $Npc1$ Hfs, both the mRNA content and protein content of ABCA1 are down-regulated (60). In addition, in macrophages, ABCA1 protein is up-regulated by cathepsin D through a posttranslational mechanism (61). Previous studies showed that blocking ACAT1 either by genetic inactivation or by using a small-molecule ACAT inhibitor increased ABCA1 protein content, with the magnitude of the enhancing effect being cell-type–dependent (62). Since we found that mutant $Npc1^{nmf}$ MEFs expressed the mature form of cathepsin D at a level significantly lower than that in the WT cells (Fig. 7*B*), we postulated that this abnormality may also cause mutant $Npc1^{nmf}$ MEFs to express ABCA1 protein at a lower level, and that $A1^{-/-}$ may be able to correct this deficiency. To test this possibility, we performed Western blot analyses in MEFs of four genotypes. As hypothesized, ABCA1 protein content in mutant $Npc1$ cells was lower than that in WT and $A1^{-/-}$ cells, whereas $Npc1^{nmf}:A1^{-/-}$ cells expressed ABCA1 protein content at level similar to that in WT cells

(Fig. 8*A*). Next, we prepared MEFs from WT and mutant mice that completely lack NPC1 (the $Npc1^{nih}$ mice) in a BALB/c genetic background and found that ABCA1 protein content in $Npc1^{nih}$ MEFs was significantly lower than that in control WT MEFs (Fig. 8*A*, compare the last two lanes). We also found that NPC1 protein content was significantly lower in mutant $Npc1^{nmf}$ cells than in WT or $A1^{-/-}$ cells (Fig. 8*A*). $A1^{-/-}$ in mutant $Npc1^{nmf}$ cells tended to increase mutant NPC1 protein content; however, the enhancing effect did not reach statistical difference. In control $Npc1^{nih}$ MEFs, NPC1 protein was completely absent. To test the in vivo implications of these findings, we performed Western blot analyses to examine the ABCA1 in homogenates prepared from cerebellum from P80 mice of four genotypes. For ABCA1 protein, the expression level in mutant $Npc1$ cerebellum was elevated over that of the WT and $A1^{-/-}$ mouse cerebellum; $A1^{-/-}$ further increased the levels of ABCA1 (Fig. 8*B*).

We next isolated the cerebellum from P50 and P90 mice of four genotypes, and monitored the mRNA levels of ABCA1 and calbindin, a protein marker for Purkinje neurons. At P50, mutant $Npc1$ cerebellum expressed lower ABCA1, and the lower expression was restored to a near normal value by $A1^{-/-}$ (Fig. 8*C*). However, at P90, both $Npc1^{nmf}$ cerebellum and $Npc1^{nmf}:A1^{-/-}$ cerebellum expressed higher ABCA1 mRNA than WT and A1$^{-/-}$ cerebellum. Overall, these results (Fig. 8*C*) are not entirely consistent with our results for ABCA1 mRNA levels in MEFs (*SI Appendix*, Fig. S2), suggesting that in vivo the effects of A1B in mutant $Npc1$ cerebellum are complex, and possibly temporal-dependent or cell-type–dependent. Control results showed that at both P50 (Fig. 8*C*) and P90 (Fig. 8*D*), NPC1^{nmf} mouse cerebellum expressed lower calbindin mRNA than WT and $A1^{-/-}$ mouse cerebellum, and $A1^{-/-}$ partially restored calbindin mRNA in the mutant NPC1 cerebellum in both ages. The latter results corroborated those described earlier (Fig. 2*D*), demonstrating that $A1^{-/-}$ partially protected Purkinje neuron loss in the mutant $NPC1$ cerebellum.

Discussion

In the present work, we genetically inactivated ACAT1 in a mouse model of NPCD and showed that $A1^{-/-}$ delays the onset of weight loss and sensorimotor impairment, ameliorates
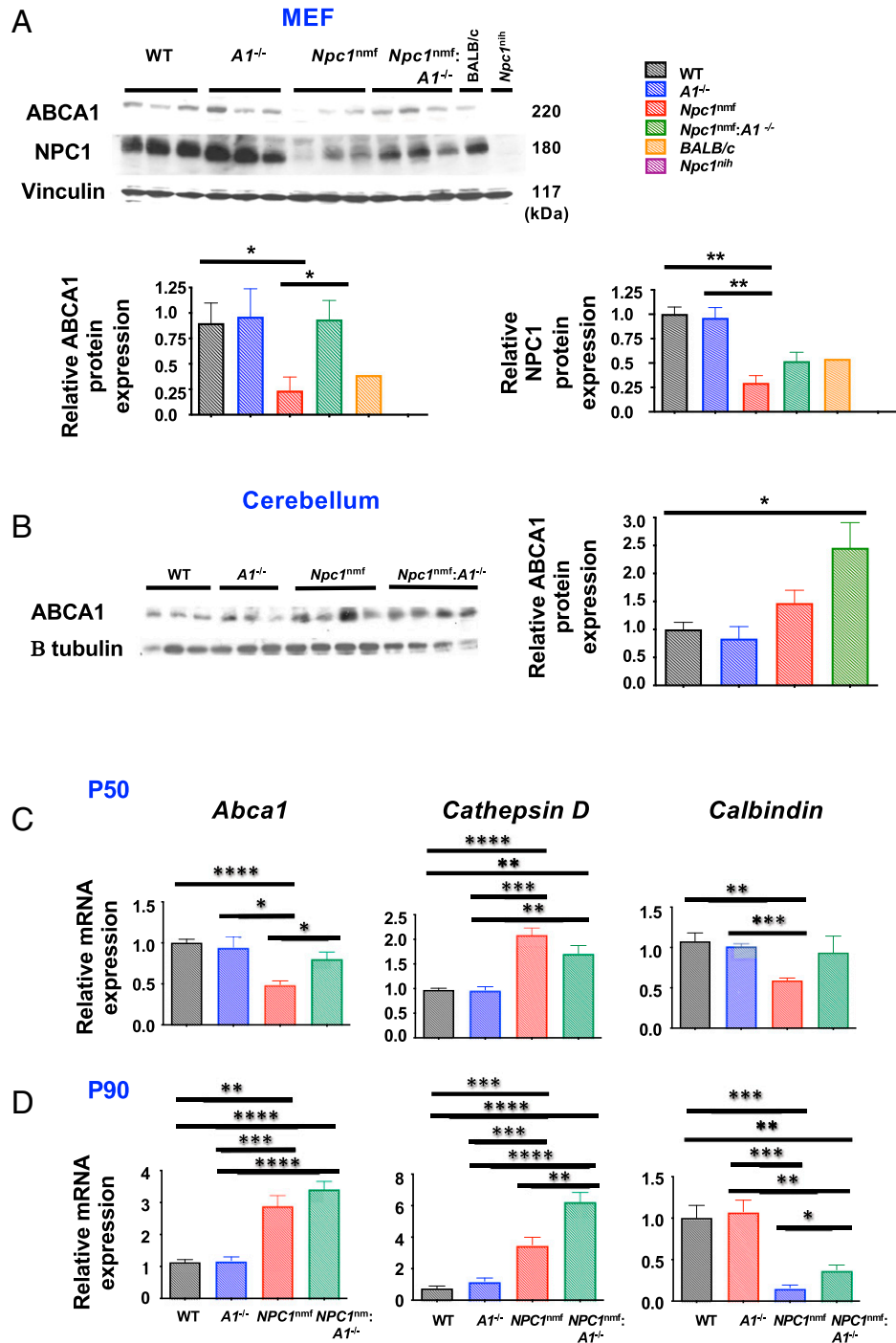
Fig. 8. (A) Relative protein contents of ABCA1 and NPC1 in various MEFs, as described in *SI Appendix, Materials and Methods*. The Western blot as shown is representative of three independent experiments. (B) Relative protein contents of ABCA1 in P80 mouse cerebellum, as described in *SI Appendix, Materials and Methods*, with one mouse per sample. The Western blot as shown is representative of two independent experiments. (C and D) Gene expressions of ABCA1 and calbindin in mouse cerebellums at days P50 (C) and P90 (D), as described in *SI Appendix, Materials and Methods*. n = 4 to 5 mice for P50 mice; n = 5 to 7 for P90 mice. *P < 0.05; **P < 0.01; ***P < 0.001; ****P < 0.0001.

certain systemic and neuropathological NPCD hallmarks, and prolongs the mean lifespan by 34%. To our knowledge, the present study is unique in demonstrating that knockout of a single gene can extend the average lifespan of a mutant *Npc1* mouse model by more than 30%. Mutant NPC cells exhibit altered cellular cholesterol distribution and display functional deficiencies in multiple membrane organelles. Here we show that in mutant NPC1 cells, A1B decreased the cholesterol accumulation associated with LE/LYS, while it increased the cholesterol contents associated with TGN and with mitochondria.

Functionally, A1B restored the normal distribution of syntaxin 6 and golgin 97 at TGN, increased ABCA1 protein content, and restored the functionality of the mannose 6-phosphate receptor pathway, which involves both the Golgi and endosome compartments. These data implicate that in mutant *Npc1* cells, A1B ameliorates the functional deficiencies of multiple organelles by altering the membrane cholesterol contents of these organelles.

It is not yet clear how blocking ACAT1, which resides at the ER, can alter the membrane cholesterol content in multiple

organelles. Recent data show that ACAT1 is enriched at the mitochondrial-associated membrane (MAM), which is a portion of the mitochondrial membrane in close physical contact with the ER membrane (63). It is possible that A1B diverts the cholesterol storage pool such that this pool moves through the MAM to mitochondria for utilization. In addition to the MAM, membrane contact sites exist between the ER membrane and membranes of several other membrane organelles, including the PM, Golgi, and endosomes. A1B may divert the cholesterol storage pool such that this pool can move to other membrane organelles through various membrane contact sites for utilization. Further investigations are needed to test these possibilities. This scenario may help to explain why in cell and mouse models, A1B is able to ameliorate Alzheimer's disease (64, 65). The concept of providing more efficient use of cholesterol by blocking cholesterol storage maybe applicable to ameliorate other neurological disorders that also involve cholesterol dys-homeostasis, such as Smith-Lemli-Opitz syndrome and autism spectrum disorder.

For antiatherosclerosis treatment, several ACAT inhibitors have completed phase I safety trials (66). For treating NPCD, however, an important preclinical evaluation will be to test their brain permeability in animal models. We are currently developing methods (67) to deliver brain-permeable ACAT inhibitors to young mutant NPC1 mice on a daily basis. On the longer time horizon, ACAT inhibitors will require testing in NPC patients without deficiency in the cellular cholesterol efflux process. In addition, as NPCD involves abnormal accumulations of both cholesterol and glycosphingolipids, a combinatorial therapy may be needed to effectively suppress the disease phenotype. To this end, mutant NPC1 mice lacking ACAT1, as reported here, can serve as a valuable tool for identification of other agents needed for a safe and effective therapeutic regimen for NPCD.

Materials and Methods

For antibodies sources, primer sequences used for RT-PCR, and methods in subcellular fractionation, lipid syntheses in intact cells, immunofluorescent staining of MEF cells, fluorescence microscopy, transfection, click chemistry, quantification of cholesterol content in various cellular compartments, measurement of long-lived proteins, and other procedures, please see *SI Appendix*.

Animal studies were conducted under Dartmouth Animal Research Center Institutional Animal Care and Use Committee–approved protocol no. 00002125.

Data Availability. All study data are included in the main text and *SI Appendix*.

Author affiliations: [a]Department of Biochemistry and Cell Biology, Geisel School of Medicine at Dartmouth, Hanover, NH 03755; [b]Department of Biology, Dartmouth College, Hanover, NH 03755; [c]Department of Biomedical Science, Centre for Membrane Interactions and Dynamics, University of Sheffield, Sheffield S10 2TN, United Kingdom; and [d]Department of Chemistry & Chemical Biology, University of New Mexico, Albuquerque, NM 87131

1. E. D. Carstea et al., Niemann-Pick C1 disease gene: Homology to mediators of cholesterol homeostasis. *Science* **277**, 228–231 (1997).
2. S. Naureckiene et al., Identification of HE1 as the second gene of Niemann-Pick C disease. *Science* **290**, 2298–2301 (2000).
3. P. G. Pentchev et al., Group C Niemann-Pick disease: Faulty regulation of low-density lipoprotein uptake and cholesterol storage in cultured fibroblasts. *FASEB J.* **1**, 40–45 (1987).
4. M. T. Vanier, Lipid changes in Niemann-Pick disease type C brain: Personal experience and review of the literature. *Neurochem. Res.* **24**, 481–489 (1999).
5. M. Pineda, M. Walterfang, M. C. Patterson, Miglustat in Niemann-Pick disease type C patients: A review. *Orphanet J. Rare Dis.* **13**, 140 (2018).
6. D. S. Ory et al., Intrathecal 2-hydroxypropyl-β-cyclodextrin decreases neurological disease progression in Niemann-Pick disease, type C1: A non-randomised, open-label, phase 1-2 trial. *Lancet* **390**, 1758–1768 (2017).
7. S. Ward, P. O'Donnell, S. Fernandez, C. H. Vite, 2-Hydroxypropyl-beta-cyclodextrin raises hearing threshold in normal cats and in cats with Niemann-Pick type C disease. *Pediatr. Res.* **68**, 52–56 (2010).
8. C. D. Davidson et al., Improved systemic AAV gene therapy with a neurotrophic capsid in Niemann-Pick disease type C1 mice. *Life Sci. Alliance* **4**, e202101040 (2021).
9. M. S. Brown, J. L. Goldstein, A receptor-mediated pathway for cholesterol homeostasis. *Science* **232**, 34–47 (1986).
10. N. Friedland, H. L. Liou, P. Lobel, A. M. Stock, Structure of a cholesterol-binding protein deficient in Niemann-Pick type C2 disease. *Proc. Natl. Acad. Sci. U.S.A.* **100**, 2512–2517 (2003).
11. N. Ohgami et al., Binding between the Niemann-Pick C1 protein and a photoactivatable cholesterol analog requires a functional sterol-sensing domain. *Proc. Natl. Acad. Sci. U.S.A.* **101**, 12473–12478 (2004).
12. R. E. Infante et al., Purified NPC1 protein. I. Binding of cholesterol and oxysterols to a 1278-amino acid membrane protein. *J. Biol. Chem.* **283**, 1052–1063 (2008).
13. S. R. Pfeffer, NPC intracellular cholesterol transporter 1 (NPC1)-mediated cholesterol export from lysosomes. *J. Biol. Chem.* **294**, 1706–1709 (2019).
14. S. R. Cheruku, Z. Xu, R. Dutia, P. Lobel, J. Storch, Mechanism of cholesterol transfer from the Niemann-Pick C2 protein to model membranes supports a role in lysosomal cholesterol transport. *J. Biol. Chem.* **281**, 31594–31604 (2006).
15. K. M. Wojtanik, L. Liscum, The transport of low density lipoprotein-derived cholesterol to the plasma membrane is defective in NPC1 cells. *J. Biol. Chem.* **278**, 14850–14856 (2003).
16. A. Das, M. S. Brown, D. D. Anderson, J. L. Goldstein, A. Radhakrishnan, Three pools of plasma membrane cholesterol and their relation to cholesterol homeostasis. *eLife* **3**, e02882 (2014).
17. K. W. Underwood, N. L. Jacobs, A. Howley, L. Liscum, Evidence for a cholesterol transport pathway from lysosomes to endoplasmic reticulum that is independent of the plasma membrane. *J. Biol. Chem.* **273**, 4266–4274 (1998).
18. X. Du et al., A role for oxysterol-binding protein-related protein 5 in endosomal cholesterol trafficking. *J. Cell Biol.* **192**, 121–135 (2011).
19. D. Höglinger et al., NPC1 regulates ER contacts with endocytic organelles to mediate cholesterol egress. *Nat. Commun.* **10**, 4276 (2019).
20. K. Zhao, N. D. Ridgway, Oxysterol-binding protein-related protein 1L regulates cholesterol egress from the endo-lysosomal system. *Cell Rep.* **19**, 1807–1818 (2017).
21. B. B. Chu et al., Cholesterol transport through lysosome-peroxisome membrane contacts. *Cell* **161**, 291–306 (2015).
22. M. Abdul-Hammed, B. Breiden, G. Schwarzmann, K. Sandhoff, Lipids regulate the hydrolysis of membrane bound glucosylceramide by lysosomal β-glucocerebrosidase. *J. Lipid Res.* **58**, 563–577 (2017).
23. M. Reverter et al., Cholesterol regulates syntaxin 6 trafficking at trans-Golgi network endosomal boundaries. *Cell Rep.* **7**, 883–897 (2014).
24. W. Yu et al., Altered cholesterol metabolism in Niemann-Pick type C1 mouse brains affects mitochondrial function. *J. Biol. Chem.* **280**, 11731–11739 (2005).
25. M. Charman, B. E. Kennedy, N. Osborne, B. Karten, MLN64 mediates egress of cholesterol from endosomes to mitochondria in the absence of functional Niemann-Pick type C1 protein. *J. Lipid Res.* **51**, 1023–1034 (2010).
26. A. Fernández, L. Llacuna, J. C. Fernández-Checa, A. Colell, Mitochondrial cholesterol loading exacerbates amyloid beta peptide-induced inflammation and neurotoxicity. *J. Neurosci.* **29**, 6394–6405 (2009).
27. C. Y. Lim et al., ER-lysosome contacts enable cholesterol sensing by mTORC1 and drive aberrant growth signalling in Niemann-Pick type C. *Nat. Cell Biol.* **21**, 1206–1218 (2019).
28. L. Liscum, R. M. Ruggiero, J. R. Faust, The intracellular transport of low density lipoprotein-derived cholesterol is defective in Niemann-Pick type C fibroblasts. *J. Cell Biol.* **108**, 1625–1636 (1989).
29. Y. Lange, T. L. Steck, The role of intracellular cholesterol transport in cholesterol homeostasis. *Trends Cell Biol.* **6**, 205–208 (1996).
30. T. Y. Chang, C. C. Chang, N. Ohgami, Y. Yamauchi, Cholesterol sensing, trafficking, and esterification. *Annu. Rev. Cell Dev. Biol.* **22**, 129–157 (2006).
31. I. Tabas, Consequences of cellular cholesterol accumulation: Basic concepts and physiological implications. *J. Clin. Invest.* **110**, 905–911 (2002).
32. J. F. Oram, J. W. Heinecke, ATP-binding cassette transporter A1: A cell cholesterol exporter that protects against cardiovascular disease. *Physiol. Rev.* **85**, 1343–1372 (2005).
33. C. C. Chang, H. Y. Huh, K. M. Cadigan, T. Y. Chang, Molecular cloning and functional expression of human acyl-coenzyme A:cholesterol acyltransferase cDNA in mutant Chinese hamster ovary cells. *J. Biol. Chem.* **268**, 20747–20755 (1993).
34. C. C. Chang et al., Regulation and immunolocalization of acyl-coenzyme A: Cholesterol acyltransferase in mammalian cells as studied with specific antibodies. *J. Biol. Chem.* **270**, 29532–29540 (1995).
35. E. Area-Gomez et al., Upregulated function of mitochondria-associated ER membranes in Alzheimer disease. *EMBO J.* **31**, 4106–4123 (2012).
36. L. Abi-Mosleh, R. E. Infante, A. Radhakrishnan, J. L. Goldstein, M. S. Brown, Cyclodextrin overcomes deficient lysosome-to-endoplasmic reticulum transport of cholesterol in Niemann-Pick type C cells. *Proc. Natl. Acad. Sci. U.S.A.* **106**, 19316–19321 (2009).
37. B. Mesmin et al., STARD4 abundance regulates sterol transport and sensing. *Mol. Biol. Cell* **22**, 4004–4015 (2011).
38. Y. Yamauchi et al., Deficiency in the lipid exporter ABCA1 impairs retrograde sterol movement and disrupts sterol sensing at the endoplasmic reticulum. *J. Biol. Chem.* **290**, 23464–23477 (2015).

39. R. A. Maue et al., A novel mouse model of Niemann-Pick type C disease carrying a D1005G-Npc1 mutation comparable to commonly observed human mutations. *Hum. Mol. Genet.* **21**, 730–750 (2012).
40. V. L. Meiner et al., Disruption of the acyl-CoA:cholesterol acyltransferase gene in mice: Evidence suggesting multiple cholesterol esterification enzymes in mammals. *Proc. Natl. Acad. Sci. U.S.A.* **93**, 14041–14046 (1996).
41. C. Y. Jao, M. Roth, R. Welti, A. Salic, Metabolic labeling and direct imaging of choline phospholipids in vivo. *Proc. Natl. Acad. Sci. U.S.A.* **106**, 15332–15337 (2009).
42. A. B. Neef, C. Schultz, Selective fluorescence labeling of lipids in living cells. *Angew. Chem. Int. Ed. Engl.* **48**, 1498–1500 (2009).
43. H. C. Kolb, M. G. Finn, K. B. Sharpless, Click chemistry: Diverse chemical function from a few good reactions. *Angew. Chem. Int. Ed. Engl.* **40**, 2004–2021 (2001).
44. K. Hofmann et al., A novel alkyne cholesterol to trace cellular cholesterol metabolism and localization. *J. Lipid Res.* **55**, 583–591 (2014).
45. J. J. Hulce, A. B. Cognetta, M. J. Niphakis, S. E. Tully, B. F. Cravatt, Proteome-wide mapping of cholesterol-interacting proteins in mammalian cells. *Nat. Methods* **10**, 259–264 (2013).
46. J. B. Bock, J. Klumperman, S. Davanger, R. H. Scheller, Syntaxin 6 functions in trans-Golgi network vesicle trafficking. *Mol. Biol. Cell* **8**, 1261–1271 (1997).
47. L. Orci et al., Heterogeneous distribution of filipin–cholesterol complexes across the cisternae of the Golgi apparatus. *Proc. Natl. Acad. Sci. U.S.A.* **78**, 293–297 (1981).
48. Y. Urano et al., Transport of LDL-derived cholesterol from the NPC1 compartment to the ER involves the trans-Golgi network and the SNARE protein complex. *Proc. Natl. Acad. Sci. U.S.A.* **105**, 16513–16518 (2008).
49. S. B. Mitchell et al., Structure of the Golgi apparatus is not influenced by a GAG deletion mutation in the dystonia-associated gene Tor1a. *PLoS One* **13**, e0206123 (2018).
50. P. A. Gleeson, J. G. Lock, M. R. Luke, J. L. Stow, Domains of the TGN: Coats, tethers and G proteins. *Traffic* **5**, 315–326 (2004).
51. S. Nishimura et al., Visualization of sterol-rich membrane domains with fluorescently-labeled theonellamides. *PLoS One* **8**, e83716 (2013).
52. S. Kornfeld, Structure and function of the mannose 6-phosphate/insulinlike growth factor II receptors. *Annu. Rev. Biochem.* **61**, 307–330 (1992).
53. T. Kobayashi et al., A lipid associated with the antiphospholipid syndrome regulates endosome structure and function. *Nature* **392**, 193–197 (1998).
54. I. G. Ganley, S. R. Pfeffer, Cholesterol accumulation sequesters Rab9 and disrupts late endosome function in NPC1-deficient cells. *J. Biol. Chem.* **281**, 17890–17899 (2006).
55. P. Benes, V. Vetvicka, M. Fusek, Cathepsin D–Many functions of one aspartic protease. *Crit. Rev. Oncol. Hematol.* **68**, 12–28 (2008).
56. J. F. Oram, ATP-binding cassette transporter A1 and cholesterol trafficking. *Curr. Opin. Lipidol.* **13**, 373–381 (2002).
57. A. Venkateswaran et al., Control of cellular cholesterol efflux by the nuclear oxysterol receptor LXR alpha. *Proc. Natl. Acad. Sci. U.S.A.* **97**, 12097–12102 (2000).
58. P. Costet, Y. Luo, N. Wang, A. R. Tall, Sterol-dependent transactivation of the ABC1 promoter by the liver X receptor/retinoid X receptor. *J. Biol. Chem.* **275**, 28240–28245 (2000).
59. S. Yokoyama et al., Calpain-mediated ABCA1 degradation: Post-translational regulation of ABCA1 for HDL biogenesis. *Biochim. Biophys. Acta* **1821**, 547–551 (2012).
60. H. Y. Choi et al., Impaired ABCA1-dependent lipid efflux and hypoalphalipoproteinemia in human Niemann-Pick type C disease. *J. Biol. Chem.* **278**, 32569–32577 (2003).
61. B. Haidar et al., Cathepsin D, a lysosomal protease, regulates ABCA1-mediated lipid efflux. *J. Biol. Chem.* **281**, 39971–39981 (2006).
62. Y. Yamauchi et al., Intracellular cholesterol mobilization involved in the ABCA1/apolipoprotein-mediated assembly of high density lipoprotein in fibroblasts. *J. Lipid Res.* **45**, 1943–1951 (2004).
63. J. E. Vance, MAM (mitochondria-associated membranes) in mammalian cells: Lipids and beyond. *Biochim. Biophys. Acta* **1841**, 595–609 (2014).
64. H. J. Huttunen, D. M. Kovacs, ACAT as a drug target for Alzheimer's disease. *Neurodegener. Dis.* **5**, 212–214 (2008).
65. Y. Shibuya, C. C. Chang, T. Y. Chang, ACAT1/SOAT1 as a therapeutic target for Alzheimer's disease. *Future Med. Chem.* **7**, 2451–2467 (2015).
66. T. Y. Chang et al., Blocking cholesterol storage to treat Alzheimer's disease. *Explor. Neuroprotective Ther.* **1**, 173–184 (2021).
67. A. L. De La Torre et al., Facile method to incorporate high-affinity ACAT/SOAT1 inhibitor F12511 into stealth liposome-based nanoparticle and demonstration of its efficacy in blocking cholesteryl ester biosynthesis without overt toxicity in neuronal cell culture. *J. Neurosci. Methods* **367**, 109437 (2022).
68. C. C. Chang, G. M. Doolittle, T. Y. Chang, Cycloheximide sensitivity in regulation of acyl coenzyme A:cholesterol acyltransferase activity in Chinese hamster ovary cells. 1. Effect of exogenous sterols. *Biochemistry* **25**, 1693–1699 (1986).